Macromolecules

Article

pubs.acs.org/Macromolecules

Surface-Initiated Polymerization by Means of Novel, Stable, Non-Ester-Based Radical Initiator

Erich D. Bain,[†] Keith Dawes,[†] A. Evren Özçam,[†,⊥] Xinfang Hu,[‡] Christopher B. Gorman,[‡] Jiří Šrogl,[§] and Jan Genzer*[,†]

[†]Department of Chemical & Biomolecular Engineering, North Carolina State University, Raleigh, North Carolina 27695, United States

[‡]Department of Chemistry, North Carolina State University, Raleigh, North Carolina 27695, United States

[§]Institute of Chemistry & Biochemistry, Academy of Sciences of the Czech Republic, Prague, Czech Republic

Supporting Information

ABSTRACT: A novel, ester-free initiator for surface-initiated free radical polymerization has been synthesized and tested. The structurally non-symmetrical azo-based initiator features a chemically stable alkane linker between the initiating group and the silane anchoring group, setting it apart from the majority of surface initiators that are linked by hydrolyzable moieties, such as esters. The novel design of the initiator is bolstered by an original synthetic approach, leading to a greater yield and a dramatic reduction in cyanide usage relative to previous methods. Here we demonstrate the capability of this novel initiator for surface-initiated free radical polymerization (SI-FRP), reverse ATRP, and RAFT, noting that Arrhenius behavior of SI-FRP differs significantly from that of FRP in the bulk. Furthermore, we show that polymer brushes formed from the novel initiator are more stable than those formed from ester-based initiators.

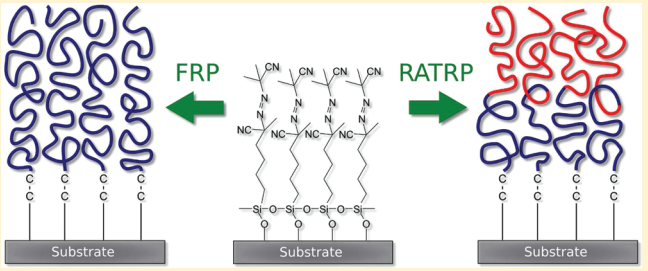

INTRODUCTION

Polymers grafted at surfaces and interfaces represent an attractive platform for a growing number of applications. These include antifouling layers for medical devices and marine craft,[1−5] biologically functionalized materials for assays and cell cultures,[6−11] and patterned responsive surfaces[12,13] that react reversibly to external stimuli, e.g., solvent,[14−17] temperature,[18−23] pH/ionic strength,[24−29] or externally applied fields.[30−32] While so-called polymer "brushes" can be formed by allowing end-functionalized bulk polymer to adsorb onto a surface with some affinity or reactivity, this approach (known as "grafting to") faces serious kinetic limitations in the density with which the chains may pack on the surface.[33−35] A further limitation to adsorption is the entropy cost associated with dense grafting; excluded volume interactions force crowded polymers into unfavorable stretched conformations that are not compensated by the modest free energy gain of the "grafting to" reaction. In order to create a densely packed brush, in which the end-tethered macromolecules are forced into the stretched conformation, a "grafting from" approach is necessary. This method involves first functionalizing a surface with a dense layer comprising small polymerization initiators and then introducing the substrate into a monomer solution to initiate polymerization from the substrate. Since the diffusion of small monomers into the grafted polymer layer is much faster than that of bulky free polymers, the kinetic limitation is overcome and very thick brushes (up to thousands of nanometers) can be formed. "Grafting from" polymerization has enjoyed tremendous popularity in the literature in the past decade, being used routinely for surface-initiated (SI) polymerizations following different mechanisms, including atom transfer radical polymerization (ATRP),[36,37] reversible addition−fragmentation chain transfer (RAFT),[38,39] and free-radical polymerization (FRP).[40−42]

FRP reactions are simple and robust. They represent one of the most industrially employed polymerization mechanisms. However, a key disadvantage of any FRP is that it produces polymers with a broad molecular weight distribution. Furthermore, polymers formed by FRP are not "living" in the sense that they cannot be reinitiated to form block copolymers or other complex architectures. While controlled radical polymerizations (CRP), e.g., ATRP or RAFT, offer relatively good control over molecular weight distribution, they require additives that increase material and purification costs and may interfere with polymerization of some monomers, i.e., methacrylic acid in the case of ATRP.[43] In contrast to SI-CRP, SI-FRP is capable of forming polymer brushes using just two basic ingredients, i.e., monomer (often in solvent), and a substrate functionalized with a suitable initiator, without any need of a catalyst. Recent computer simulation studies have cast doubt on the ability of surface-initiated CRP to form

Received: March 9, 2012
Published: April 25, 2012

monodisperse polymer brushes due to confinement effects among propagating chains.[44−46] SI-FRP therefore remains a viable alternative for efficient brush formation in applications where complex polymer architectures are not required. For example, SI-FRP is a simple route to form stimuli-responsive mixed brush layers consisting of dissimilar homopolymers.[47−49]

An overwhelming majority of initiators used for surface-initiated polymerization methods contain cleavable functional groups, such as esters, between the headgroup, which anchors the molecule to the substrate, and the tail group that initiates polymerization.[50−53] The long-term stability of densely packed brushes produced from such initiators is compromised because esters are susceptible to hydrolysis under relatively mild conditions. In the most common SI-ATRP initiators, the ester functionality is essential; it acts as an electron-withdrawing group that stabilizes the radical formed at the surface where polymerization is initiated. In contrast, while most common surface free radical initiators contain esters or other hydrolyzable groups, these are nonessential to the function of the initiator and can in principle be eliminated without affecting polymerization performance. Free-radical initiators, while often used for SI-FRP, have the added advantage that they may be used to initiate certain CRP mechanisms, including reverse ATRP (RATRP)[54] and RAFT.[39]

The two major classes of thermally activated free-radical initiators are based on peroxide[55−58] and azo chemistries. Most surface initiators of the azo family are structurally similar to azobis(isobutyronitrile) (AIBN),[59,60] while semiaromatic azo monolayers whose structure and kinetics differ slightly from those of AIBN have been used successfully for photoinitiated SI-FRP.[61,62] Many SI-FRP studies employ symmetrical azo molecules, e.g., azobiscyanopentanoic acid, attached to surfaces via silane coupling chemistry.[63−65] However, the symmetrical initiator approach suffers from limitations including inconsistent grafting density and reduced efficiency due to recombination of the pair of closely linked radicals generated in each decomposition step. To overcome these limitations, Prucker and Rühe[41] synthesized an non-symmetrical AIBN-like surface initiator, in which only one generated radical remains bound to the substrate while the other initiates polymerization in the bulk, forming an untethered polymer. Their initiator forms self-assembled monolayers on silicon oxide surfaces via anchoring chlorosilane head groups, which are attached via an ester linkage to the azo complex. While this type of initiator has been utilized successfully in several SI-FRP studies,[39,54,66,67] there are certain limitations that preclude its widespread use. First, the synthesis of the azo initiator in question is synthetically complex and relatively hazardous, involving multiple synthetic steps and rather large quantities of potassium cyanide. In addition the resultant yield is rather low, i.e., ≈10.5%. Finally, the presence of the ester-based linker, while useful as a means of intentionally degrafting the chains for analysis, may pose challenges regarding the stability of the grafted polymer layer in practical applications because ester bonds are unstable under moderate pH conditions and are thus susceptible to scission as mentioned above.

Here, we describe the synthesis of a novel unsymmetrical azo initiator featuring a simple alkyl linker between an AIBN-like tail group and a chlorosilane anchoring headgroup. The initiator is an attractive choice for brush formation in applications where stability is a prerequisite because it does not contain easily hydrolyzable functional groups. The synthetic yield of the initiator is >20% (i.e., double that of previous methods), and cyanide usage in practice is reduced by more than 70% relative to the previous method. We refer to the novel initiator as BAIN, in recognition of the primary author of this study while making a parallel to the conventional bulk initiator AIBN. We demonstrate the use of BAIN for forming polymer brushes by SI-FRP, and we investigate the Arrhenius behavior of SI-FRP compared against simulations of FRP in solution. We compare BAIN to two different Rühe-type azo initiators, including azo ester trichlorosilane (AETS) and azo ester monochlorosilane (AEMS), which has a dimethylchlorosilane anchoring group. We illustrate the versatility of BAIN by showing that it can be used for surface-initiated controlled radical polymerizations including RATRP and RAFT. Finally, we present evidence that polymer brushes formed from the BAIN initiator are more stable than those formed from ester-based initiators, both under harsh conditions typically used for brush cleavage and under milder conditions where tension due to interchain interactions can accelerate degrafting of ester-based polymers.

PROCEDURES AND METHODS

Materials. Acetone, hydrazine hydrate, potassium hydroxide, 5-hexen-2-one, trimethylsilyl cyanide, diethyl ether, sodium sulfate, lead tetraacetate, trichlorosilane, platinum(0)−1,3-divinyl-1,1,3,3-tetramethyldisiloxane complex (3 wt % solution in xylenes), toluene, anisole, copper(I) bromide, copper(II) bromide, *N*,*N*,*N*′,*N*′,*N*″-pentamethyldiethylenetriamine (PMDETA), 2,2′-bipyridyl, azobis(isobutyronitrile) (AIBN), 2-cyano-2-propyldodecyltrithiocarbonate, *p*-toluenesulfonic acid, dimethylformamide (DMF), copper(I) chloride, copper(II) chloride, and *p*-toluenesulfonic acid were purchased from Sigma-Aldrich and used as received. Silicon wafers with 150 mm diameter, 675 ± 25 μm thickness, ⟨100⟩ orientation, and 1−30 ohm·cm resistivity were purchased from Silicon Valley Microelectronics. Phosphate buffered saline 1X solution was purchased from Fisher Scientific and used as received.

Anhydrous hydrazine (Aldrich) was stored over barium oxide overnight for additional drying. Deionized water (resistivity 15 MΩ·cm) was produced by a Millipore filtration system. Anhydrous chloroform and anhydrous toluene were formed by standing ACS grade chloroform (Aldrich) and toluene (Aldrich), respectively, over activated 4 Å molecular sieves (Aldrich). Anhydrous dichloromethane was formed by shaking ACS grade dichloromethane (Aldrich) over calcium hydride (Aldrich) and distilling onto activated molecular sieves. Triethylamine was shaken over potassium carbonate (Aldrich) and distilled onto activated molecular sieves. Styrene (Aldrich) was passed through a column of basic alumina (Aldrich) to remove the inhibitor, 4-*tert*-butylcatechol. Methyl methacrylate and 2-(dimethylamino)ethyl methacrylate (Aldrich) were each passed through a column of inhibitor remover resin (Aldrich) to remove hydroquinone monomethyl ether (MEHQ). The ester-containing unsymmetrical azo initiators AETS and AEMS were synthesized according to the procedure of Prucker and Rühe,[41] with a total spacer length of three carbons between the ester and the silane. [11-(2-Bromo-2-methyl)propionyloxy] undecyltrichlorosilane (BMPUS) was synthesized according to the method of Matyjaszewski and co-workers.[36]

Instrumentation. The NMR spectra were recorded on 300 MHz Gemini 2300 NMR spectrometer using $CDCl_3$ as solvent. Transmission FT-IR spectra were recorded on a ThermoNicolet 6700 using thin films on KBr crystals with a resolution of 4 cm^{-1}. Thickness values were determined by a variable angle spectroscopic ellipsometer from J.A. Woollam Co. via the following procedure: Ellipsometric data for initiator layers were recorded at an incident angle of 75° and a wavelength range of 400−1000 nm, while for polymer brush layers an incident angle of 70° and a wavelength range of 500−1100 nm were used. The ellipsometric data, consisting of the angles Ψ and Δ, depend on thickness and dielectric constant of the organic layer on the

Scheme 1. Synthesis of BAIN, Novel Surface-Attaching Radical Initiator with Alkyl Linker between AIBN-like Tail Group and Trichlorosilane Anchoring Group

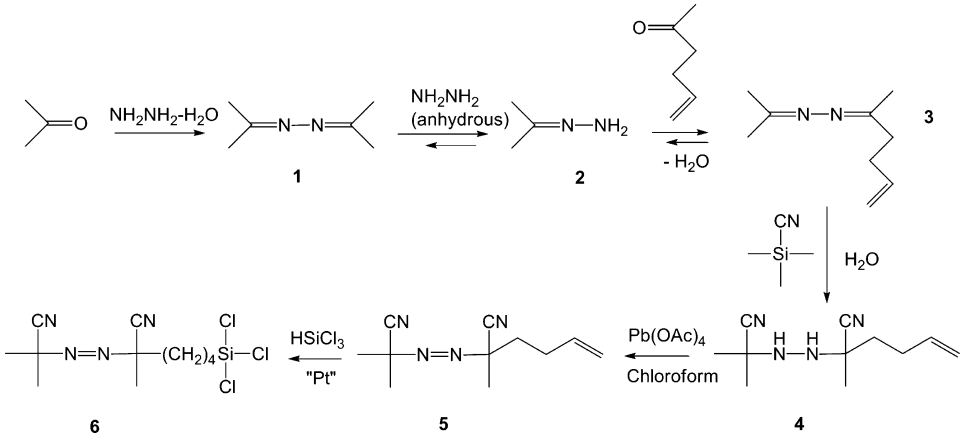

substrate. For polymer brush layers the best fit to the data was obtained by varying optical constants and thickness, but for very thin films these parameters are highly correlated and cannot be decoupled.[68] Therefore, to fit thickness of the initiator layers, we assumed a constant refractive index $n = 1.5$, noting that a difference in n of ± 0.05 corresponds to an uncertainty of approximately ± 0.1 nm.[69,70] The fitting model in all cases assumed a layer of silicon oxide below the grafted layer with a thickness of 1.5 nm and refractive index of 1.462. Reported thicknesses represent averages of measurements on at least three spots per sample, with the standard deviation given as the error. Water contact angles (WCA) were measured using a Ramé-Hart NRL goniometer (model 100-10). To measure the advancing contact angle, an 8 μL drop of DI water was added onto the surface by means of a syringe. To measure the receding contact angle, 4 μL was removed from the drop, and it was allowed to equilibrate. Reported WCA values are an average of measurements on at least three spots per sample, with the standard deviation given as the error. X-ray photoelectron spectroscopy (XPS) was measured on a Kratos Axis Ultra DLD X-ray photoelectron spectrometer using a monochromatic Al Kα source at takeoff angles of 30° and 90°, with charge neutralization turned on. Differential scanning calorimetry was measured using a TA Instruments Q100 with a heating rate of 5 °C/min under nitrogen. Size-exclusion chromatography was recorded using a Waters 2695 separations module with Waters styragel columns, toluene as the solvent, and differential refractive index recorded by a Wyatt Optilab rex.

Synthesis of Initiator. The synthetic route leading to the alkyl-linked azo initiator BAIN is depicted in Scheme 1. The details of the individual steps in the synthesis are described below. IR spectra are plotted in Figure S2 in the Supporting Information, and ^{1}H NMR spectra are plotted in Figure S3 in the Supporting Information.

Acetone Azine ***1.*** Acetone azine and acetone hydrazone were synthesized according to the literature procedure.[71] Acetone (183.0 mL, 2.50 mol) was cooled with an ice bath in a round-bottom flask. Hydrazine hydrate (63.7 mL, 1.31 mol) was added dropwise over 20–30 min with vigorous stirring, such that the temperature stayed below 35 °C. After complete addition, the solution was stirred for 20 min; then KOH pellets (50.0 g, 0.891 mol) were added with continued stirring and cooling, forming two liquid phases. The upper phase was separated and stood over fresh KOH pellets (25.0 g, 0.446 mol) for 30 min with occasional swirling, then decanted through a plug of glass wool, and dried three more times over KOH pellets (3 × 12.5 g, 0.223 mol) for 30 min each. The liquid was decanted into a round-bottom flask and distilled under nitrogen, yielding the desired product **1** as a clear, colorless liquid (120.6 g, 1.075 mol, 86% yield); bp 128–133 °C. IR (KBr): 2926, 1696 cm^{-1}. ^{1}H NMR ($CDCl_3$ in ppm): 2.0 and 1.82 (s, 6H each, CH_3).

Acetone Hydrazone ***2.*** **1** (11.20 g, 0.100 mol) and anhydrous hydrazine (3.13 mL, 0.100 mol) were each pretreated by standing over barium oxide for 4 h and then filtered and mixed in a dry round-bottom flask equipped with an air condenser capped by a drying tube. The mixture was heated at 100 °C behind a protective screen for 17 h and then quickly distilled under nitrogen, yielding the desired product **2** as a clear, colorless liquid (11.46 g, 0.159 mol, 80% yield); bp 121–126 °C. ^{1}H NMR ($CDCl_3$ in ppm): 5.0–4.7 (s, 2H, NH_2), 1.91 and 1.75 (s, 6H each, CH_3).

1-(Hex-5-en-2-ylidene)-2-(propan-2-ylidene)hydrazine ***3.*** Immediately after distillation, **2** (11.46 g, 0.159 mol) was added dropwise to 5-hexen-2-one (16.40 g, 0.166 mol) over several minutes with vigorous stirring. The vessel was cooled with a water bath and allowed to stir for 2 h. KOH pellets (6.0 g, 0.11 mol) were added and allowed to dissolve, while the flask was cooled with an ice bath. Two liquid phases formed; the top phase was separated and stood over fresh KOH pellets (3.0 g, 0.05 mol) for 30 min, decanted off, and stood over fresh KOH pellets (3.0 g, 0.05 mol) for another 30 min. The liquid was decanted into a round-bottom flask and subjected to fractional distillation at 12 mmHg. The first fraction, boiling at 25–36 °C, contained acetone azine. The second fraction, boiling at 67–74 °C, contained the desired product **3**. The remaining pot liquor was found to boil at 84–107 °C and contained the symmetric azine 1,2-di(hex-5-en-2-ylidene)-hydrazine (cf. Figure S1, **III** in the Supporting Information). The second fraction, consisting of **3**, was obtained as a clear, light yellow liquid (10.63 g, 0.070 mol, 44% yield). IR (KBr): 3077, 2979, 2917, 1642 cm^{-1}. ^{1}H NMR ($CDCl_3$ in ppm): 5.6–6.0 (m, 1H, =CH–), 4.9–5.1 (m, 2H, CH_2=), 2.3–2.4 (m, 4H, CH_2CH_2), 2.0 (m, 3H, CH_3), 1.77–1.81 (m, 6H, CH_3).

Cyanation To Form (R)-2-(2-(2-Cyanopropan-2-yl)hydrazinyl)-2-methylhex-5-enenitrile ***4.*** **3** (8.00 g, 0.0525 mol) was mixed with deionized water (2.40 mL, 0.133 mol) in a round-bottom flask and cooled in an ice bath while stirring for 30 min. Via a syringe through a septum reinforced with copper wire, trimethylsilyl cyanide (14.75 mL, 0.111 mol) was added dropwise over 5 min. No pressure was felt through the septum. The suspension was kept at 0 °C overnight, then warmed to room temperature, extracted with diethyl ether, and washed once each with water, saturated solution of sodium bicarbonate, and brine. The product was dried with sodium sulfate and concentrated under vacuum to yield a clear, colorless liquid containing **4** and a residue from the trimethylsilyl groups left over after cyanation (about 14 g total), which was used in subsequent reaction steps without further purification. IR (KBr): 3700–3200, 3273, 3078, 2988, 2939, 2228, 1642 cm^{-1}. ^{1}H NMR ($CDCl_3$ in ppm): 5.7–6.0 (m, 1H, =CH–), 4.9–5.2 (m, 2H, CH_2=), 3.6–3.7 (m, 2H, –NH–NH–), 2.2–2.4 (m, 4H, CH_2CH_2), 1.44–1.47 (m, 9H, CH_3).

Oxidation To Form (R)-2-((2-Cyanopropan-2-yl)diazenyl)-2-methylhex-5-enenitrile ***5.*** Lead(IV) acetate (5.92 g, 0.0134 mol) was added to a dry 250 mL round-bottom flask in a water bath. Anhydrous chloroform (40 mL) was added with stirring to form a light yellow solution. The cyanation product mixture (1.83 g) was dissolved in 40 mL of anhydrous chloroform and added to the solution via

syringe, causing a white precipitate to form. The solution remained light yellow while stirring for 1 h. Deionized water (70 mL) was added, causing formation of a thick reddish-brown precipitate. The mixture was filtered through Celite and then washed with water, saturated solution of sodium bicarbonate, and brine. The liquid was concentrated under vacuum, causing a small amount of bulk initiator AIBN (0.25 g) to precipitate as a white crystalline solid, which was removed by filtration in cold diethyl ether. After concentrating the filtrate, the desired product **5** was obtained as a clear, light yellow liquid (0.95 g, 0.0047 mol, ~68% overall yield for both the cyanation and oxidation steps). IR (KBr): 3080, 2991, 2938, 2243, 1747 (strong), 1643 cm^{-1}. ^1H NMR ($CDCl_3$ in ppm): 5.7−6.0 (m, 1H, =CH−), 4.9−5.2 (m, 2H, CH_2=), 2.0−2.3 (m, 4H, CH_2CH_2), 1.69−1.75 (m, 9H, CH_3).

Hydrosilylation To Form (R)-2-((2-Cyanopropan-2-yl)diazenyl)-2-methyl-6-(trichlorosilyl)hexanenitrile ***6.*** Trichlorosilane (30.0 mL, 0.30 mol) was added to **5** (0.950 g, 4.65 mM) in a round-bottom flask with stirring. Three drops of platinum(0)−1,3-divinyl-1,1,3,3-tetramethyldisiloxane complex (3 wt % solution in xylenes) was added, and the solution was heated to reflux under nitrogen for 3 h. The remaining trichlorosilane was then removed by distillation, and the concentrated product was dissolved in anhydrous dichloromethane. The solution was filtered through a column of anhydrous sodium sulfate to remove the platinum catalyst, and the solvent was removed under vacuum to yield the desired product **6** (BAIN) as a clear, orange, viscous liquid (1.40 g, 0.0041 mol, 89% yield). Anhydrous toluene (32.5 mL) was added under nitrogen to form a 5 wt % BAIN solution, which was stored in a freezer in nitrogen-purged vials.

Deposition of Initiators onto Silicon Oxide Substrates. Silicon wafers were cut into 1 × 2 cm^2 pieces, rinsed with methanol, and treated with UV-ozone for 10 min to create a hydroxyl-rich layer on the surface. The wafers were then immersed in a solution containing 5% initiator solution (80 μL) and anhydrous toluene (40 mL). Some solutions contained a few drops of pyridine or anhydrous triethylamine as a catalyst. The solution was kept in a freezer for 18 h at −12 °C. The wafers were then rinsed with toluene and dried with a stream of nitrogen gas.

Surface-Initiated Free-Radical Polymerization (SI-FRP) of Styrene. Pure styrene and toluene were each bubbled with nitrogen for at least 45 min with stirring. They were added in equal volume to nitrogen-purged vessels each containing a stir bar and a silicon wafer functionalized with azo initiator. The vessels were held at fixed temperature in a heating bath for varying times, after which the substrates were removed, rinsed with toluene, and dried under a stream of nitrogen.

Simultaneous Bulk and Surface-Initiated Reverse Atom Transfer Radical Polymerization (RATRP) of Styrene. A stock solution containing copper(II) bromide (22.3 mg, 0.100 mmol), PMDETA (26.0 mg, 0.150 mmol), and anisole (20 mL) was sonicated for 1 h to dissolve. 2 mL of the resulting solution, along with 1 mL of a stock solution containing AIBN (13.6 mg, 0.083 mmol) in anisole (10 mL), was mixed with styrene (10.0 mL, 0.087 mol) and anisole (10.0 mL) in a Schlenk flask (the final concentrations were 3.77 M styrene, 0.43 mM $CuBr_2$, 0.65 mM PMDETA, and 0.357 mM AIBN). Silicon wafers functionalized with azo initiator were added to the solution, and it was degassed by three freeze−pump−thaw cycles. Under continuous argon purge the flask was heated at 100 °C for 23 h. The substrates were then removed, rinsed with methanol, water, and toluene, and dried with nitrogen gas.

ATRP of Methyl Methacrylate from Styrene Macroinitiator Brush. Styrene brushes formed by reverse ATRP were stored in air at room temperature, away from light, for 3 h. Meanwhile, copper(I) bromide (23.8 mg, 0.166 mmol) and PMDETA (57.2 mg, 0.330 mmol) were dissolved in anisole (8.6 mL) under nitrogen and sonicated 30 min to dissolve. Methyl methacrylate (6.4 mL, 0.06 mol) was added, and the solution was degassed by three freeze−pump−thaw cycles. The PS macroinitiator brush samples were added to the solution, and the flask was heated to 100 °C for 24 h under continuous argon purge. The samples were subsequently rinsed with toluene, methanol, and water, sonicated in a 4:1 mixture (by volume) of chloroform/methanol, a 1:1 mixture (by volume) of water/methanol, rinsed with toluene, and dried with nitrogen gas.

Surface-Initiated Reversible Addition−Fragmentation Transfer (SI-RAFT) Polymerization. Styrene and toluene were each bubbled with nitrogen for 1 h, mixed in a 1:1 ratio (v/v), and degassed by three freeze−pump−thaw cycles. This solution was transferred under argon purge to vials containing silicon wafers functionalized with initiator, and varying amounts of 2-cyano-2-propyl-dodecyltrithiocarbonate were added. The vials were heated at 70 °C for 18 h, and then the substrates were rinsed with toluene, sonicated in toluene, and dried with nitrogen gas.

Treatment of SI-FRP Polystyrene Brushes with *p*-Toluenesulfonic Acid. Silicon wafers coated with polystyrene brushes formed by SI-FRP were placed in crimp-top vials containing a stir bar. Portions of a solution containing *p*-toluenesulfonic acid monohydrate (10 mg, 53 μmol) in toluene (20 mL) and methanol (2 mL) were added. The vials were sealed and heated to reflux (about 100 °C) overnight, after which the samples were removed, rinsed with toluene, and dried under a stream of nitrogen. Thickness after the treatment was measured by VASE.

SI-FRP of 2-(Dimethylamino)ethyl Methacrylate (DMAEMA). Silicon wafers functionalized with BAIN were placed in glass vials containing a mixture of DMAEMA and DMF (1:1 v/v). The polymerization mixture was degassed by bubbling with nitrogen for at least 45 min, after which the vials were sealed and placed in an oil bath at 80 °C for ≈20 h, resulting in 100% initiator conversion. Following SI-FRP, the silicon wafers were taken out of the vials, washed with acetone to remove any free polymer, sonicated for 2 + 2 min in acetone, rinsed with acetone, and dried under a stream of nitrogen gas.

SI-ATRP of 2-(Dimethylamino)ethyl Methacrylate (DMAEMA). [11-(2-Bromo-2-methyl)propionyloxy]undecyltrichlorosilane (BMPUS) was deposited on silicon substrates as described above, and the silicon wafers were placed in glass vials. DMAEMA (31.10 g, 0.198 mol) was mixed with of DI water (6.67 g), methanol (0.45 g), and 2,2′-bipyridyl (2.00 g, 12.8 mmol) in an argon-purged Schlenk flask, and oxygen was removed via three freeze−pump−thaw cycles. After removal of oxygen, CuCl (0.63 g, 6.36 mmol) and $CuCl_2$ (0.04 g, 0.298 mmol) were added to the solution, and one more freeze−thaw cycle was performed. The ATRP polymerization mixture was transferred to the glass vials containing the initiator-coated silicon wafers, and the vial was sealed under argon at room temperature. The polymerization was stopped after ≈12 h by exposing the reaction mixture to oxygen. The wafers were washed with acetone, sonicated in acetone (2 + 2 min), rinsed with acetone, and dried under a stream of nitrogen gas.

Quaternization of the Amine Groups in PDMAEMA Brushes. PDMAEMA brush samples were heated in a solution of iodomethane in acetonitrile at 60 °C for ≈20 h. An excess amount of iodomethane was used to ensure fully quarternized q-PDMAEMA brushes. The quarternized samples were washed with copious amounts of acetone and dried with a stream of dry nitrogen.

Aqueous Stability Studies of PDMAEMA and q-PDMAEMA Brushes. The pH of PBS 1X solution (0.137 M NaCl, 0.0027 M KCl, and 0.0119 M phosphates) was adjusted to values of 4, 7.4, and 9 by titration with 1 M solutions of HCl and NaOH. Silicon wafers coated with PDMAEMA or qPDMAEMA brushes, whose thickness had been measured by VASE, were placed in 20 mL scintillation vials, and the vials were filled with the PBS buffer solutions at different pH values. Silicon wafers were taken out of the solutions every ≈24 h, rinsed with DI water, and dried with a stream of nitrogen gas. The resulting thicknesses of PDMAEMA and qPDMAEMA brushes were measured with VASE at approximately the same position as before.

Computer Simulation of Solution FRP by Gillespie's Stochastic Simulation Algorithm (GSSA). Computer simulations were performed according to the method of Lu et al.[72] Rate constants, molecular weights, and molar volumes were chosen to represent free-radical polymerization of styrene in toluene.[73,74] Chain transfer was neglected. The system consisted of 1 × 10^8 monomer molecules

Table 1. Properties of Azo Initiator Monolayers Grafted on Silicon Wafer Substrates

	BAIN	AEMS	AETS	AIBN
advancing water contact angle (deg)	75 ± 2	63 ± 10		
contact angle hysteresis (deg)	2	5		
av thickness (nm)	2.5 ± 0.5[a]	1.8 ± 0.7[a]	1.6 ± 0.2[a]	
XPS N 1s signal (90°, sp1)	5.57		3.84	
grafting density (nm^{-2})	9.1 ± 1.8[b]		5.0 ± 0.9[b]	
activation energy (kJ/mol)	130 ± 11[c]		133 ± 18[c]	129 ± 5[d]
ln A (1/s) (preexponential factor)	35.3 ± 3.6[c]		36.4 ± 5.9[c]	35.5 ± 1.9[d]
av PS growth rate by RATRP (nm/h)	0.9		1.3	
av PS growth rate by RAFT with 0.2 mM CTA (nm/h)	3.4			

[a]Calculated from model fits to ellipsometry data. [b]Estimated from XPS surface scans for C 1s, O 1s, N 1s, and Si 2p. [c]Estimated from fits of DSC data; see Figure 1 for BAIN. [d]Average of reported values from ref 73.

(assuming a concentration of 1 M) and 1 × 10^5 AIBN initiator molecules.

RESULTS AND DISCUSSION

Initiator Synthesis. Scheme 1 depicts the synthetic steps involved in the formation of the unsymmetrical BAIN radical initiator. The synthesis consists of six steps and results in a simple structure containing only C−C bonds between an azo initiator group and the trichlorosilane headgroup that links the initiator to an oxide surface. To the best of our knowledge, this is the first AIBN-like initiator containing only carbon−carbon bonds linking the initiator to a surface, and one of the few surface initiators of any kind to be linked by only C−C bonds.[50−53] Given the susceptibility of esters and other carbonyl-based functional groups to hydrolysis, particularly under the tension of supporting a dense macromolecular brush in an unfavorable stretched conformation, the BAIN initiator is expected to yield brushes that are more stable than those produced by most other initiators, especially in cases where brushes are charged, branched, or otherwise under tension. We show data demonstrating these effects at the end of this paper and provide a more comprehensive discussion in a separate publication.[75]

In our experiments we achieved an overall synthetic yield of 18% for the BAIN initiator. Taking literature yields for known reaction steps, the theoretical yield is ≈23% and can likely be improved by further optimization. Therefore, the new synthesis also represents a significant gain in efficiency over the previous method of synthesizing structurally unsymmetrical azo initiators, whose theoretical yield is only 11%. In addition to doubling previous yields, the novel synthesis scheme uses far less cyanide than previous methods because the efficient cyanation reaction is performed in an independent reaction step separate from the lowest yielding step. Therefore, much less cyanide is required than in the previous method, in which cyanation had been performed simultaneously with the lowest yielding step, wasting the majority of cyanide on discarded side products. To understand the implication of this improvement, suppose a research group uses 70 mM of surface azo initiator per month, a typical amount required for preparation of polymer-functionalized nanoparticles. To meet these demands by the previous synthetic method, assuming the maximum theoretical yield, would require a monthly reaction involving 87 g of potassium cyanide in a 1.3 L aqueous solution at 50 °C. In contrast, synthesizing the same amount of BAIN by the novel method requires only 24 g of trimethylsilyl cyanide (equivalent to 16 g of KCN) in a 57 mL solution at 0 °C. This corresponds to a 72% reduction in cyanide usage by mass and an even more dramatic reduction in the volume of the cyanide solution. Combining these considerations with the additional benefit of lower temperature, it is clear that the novel synthetic route is safer and more feasible for scientists who wish to regularly form polymer brushes by radical polymerization.

Deposition of Initiators on Substrates. Initiators were deposited on silicon oxide-covered silicon wafers by incubating the substrates in a dilute solution of the initiator in anhydrous toluene at −12 °C. In some cases a few drops of a basic catalyst (triethylamine or pyridine) were used to facilitate the initiator coupling to the surface. In general, we observed no effect of the catalysts on the properties of the initiator layers or the subsequent polymerization process. Therefore, in the polymerization experiments discussed in this paper we used no catalyst during the initiator deposition. Table 1 lists various properties of the initiator layers deposited on silicon wafers, including BAIN, AEMS, and AETS. The thickness of BAIN on silicon wafers as measured by ellipsometry was 2.5 ± 0.5 nm. Based on the estimated thickness of a monolayer (1.1 nm),[76] this result suggests that BAIN forms bilayers or other stacked structures in our samples. AETS (thickness 1.6 nm) and AEMS (thickness 1.8 nm) layers were closer to their estimated monolayer thickness of 1.5 nm, suggesting that they formed monolayers. These results reveal that the deposition conditions used in this study are not ideal for BAIN. Nevertheless, advancing DI water contact angles of BAIN layers were 74 ± 3°, with a contact angle hysteresis of 4°, indicating a relatively smooth layer. The average water contact angle of AEMS was slightly lower than that of BAIN, presumably owing to smaller coverage of the silicon oxide surface, as well as possible partial exposure of the ester groups at the surface. The grafting densities of BAIN and AETS were assessed by XPS surface scans, based on a least-squares analysis of XPS signals for carbon, oxygen, nitrogen, and silicon. Representative XPS spectra are shown in Figure S4 in the Supporting Information. The calculated grafting density of BAIN was nearly double that of AETS, which agrees with the hypothesis discussed above that the novel initiator forms bilayers under these conditions.

Thermal Decomposition of Initiators. The kinetics of the initiator decomposition were characterized using differential scanning calorimetry (DSC) measured on the neat, unbound initiators. The DSC trace of pure BAIN is shown in Figure 1a. The Arrhenius constants for the initiator decomposition can be obtained from a single DSC trace as follows:[77] The heat of reaction ΔH_{tot} is calculated by integrating the dH/dt curve (appropriately zeroed to the baseline value) as a function of temperature and dividing by the heating rate (°C/time). The reaction conversion $x(T)$ at each temperature is then evaluated

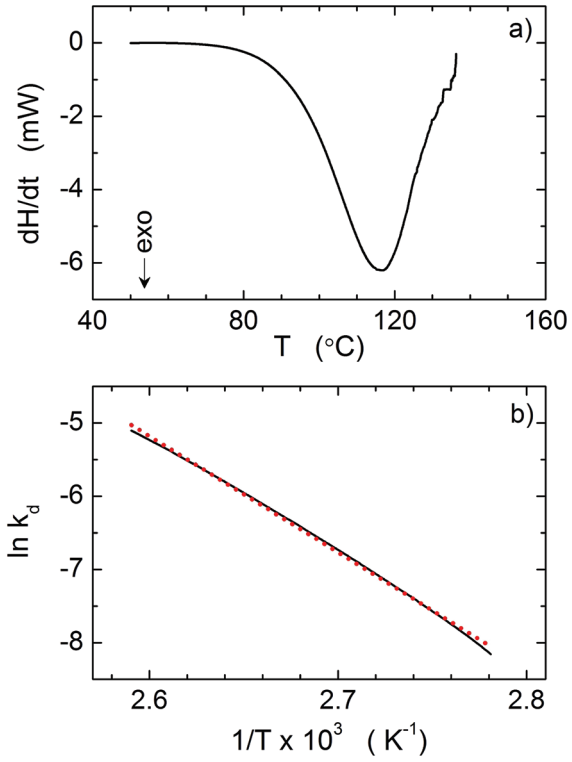

Figure 1. (a) DSC trace of BAIN with 5 °C/min heating rate. (b) Linear portion of Arrhenius plot derived from DSC trace in (a). The red dotted line denotes the best linear fit to the data.

by integrating the heat evolved up to that point ΔH_i and dividing by the total heat of reaction ΔH_{tot}. The rate constant k_d of initiator decomposition, assuming a first-order reaction, is given by eq 1:

$$k_d(T) = \frac{dH}{dT}\frac{1}{\Delta H_{tot}(1 - x(T))} \quad (1)$$

Once a k_d value has been calculated for each temperature, an Arrhenius plot in the form of ln k_d vs $1/T$ (K) can be generated. The linear portion of the plot, typically the values between 1% and 50% of initiator conversion, are fitted to a line, and the slope and intercept are used to determine the activation energy and the pre-exponential factor, respectively. Figure 1b shows the Arrhenius plot derived from the DSC trace for BAIN. The activation energy was determined to be ≈130 kJ/mol, which along with the preexponential factor $\approx 10^{15}$ s^{-1} is in good agreement with the kinetic data for the ester-based azo initiator and AIBN.[42,73] DSC was also used to measure the decomposition kinetics of AETS by the same procedure, giving similar results as seen in Figures S5 and S6 in the Supporting Information. The activation energy and preexponential factor for BAIN, AETS, and AIBN are compared in Table 1.

Surface-Initiated Free Radical Polymerization (SI-FRP). To form polystyrene brushes by SI-FRP, we heated BAIN-functionalized silicon wafers in degassed solutions of styrene (4.35 M) in toluene. Based on the kinetics of decomposition discussed above, the approximate time needed to reach various BAIN initiator conversions at five different temperatures was calculated and is shown in Table 2. One BAIN-functionalized silicon wafer was heated at each of the time/temperature combinations listed in Table 2; the resulting polymer

Table 2. Polymerization Time (hours) To Reach Desired Conversion of BAIN at Various Temperatures

	BAIN initiator conversion				
T (°C)	50%	70%	90%	99%	100%
75	2.5	4.3	8.3	16.4	43.2
85	0.7	1.2	2.3	4.7	12.3
93	0.3	0.6	0.9	1.8	4.8
100	0.1	0.2	0.4	0.8	2.1
105		0.1	0.2	0.5	1.2

thicknesses were measured using spectroscopic ellipsometry. Figure 2a summarizes the results from these measurements.

As a basis of comparison, we performed computer simulations of bulk free radical polymerization of styrene in toluene using the Gillespie's stochastic simulation algorithm (GSSA) as described by Lu et al.[72] The pre-exponential factors and activation energies for rate constants used in the model are given in Table 3. The GSSA is useful for studying complex systems of reactions that are not easily solved with differential rate equations. It has particular advantages for FRP, including that it is capable of calculating the full molecular weight distribution, and it does not rely on the steady state approximation. However, GSSA is not well suited to simulating surface-initiated polymerization because it assumes a homogeneous spatial distribution of reacting species and does not account properly for confinement effects.[78] Therefore, we present simulations of bulk polymerization only, with the following caveat: the GSSA bulk simulation results in this section are neither intended as a quantitative prediction of the molecular weight of the surface-grafted polymer nor as a means of estimating polymer grafting density, but only as a guide for qualitative comparison of the SI-FRP results. In general, surface and bulk polymer molecular weight tend to differ due to effects of confinement on the polymerization process. For example, Monte Carlo simulations of simultaneous bulk and surface-initiated CRP indicate that under certain conditions surface-initiated polymers tend to grow slower, to smaller molecular weights, and have broader polydispersity, than their counterparts in the bulk.[46] We represent the discrepancy between bulk and surface polymers generally as follows:

$$M_{n,s} = \xi M_{n,b} \quad (2)$$

where $M_{n,s}$ and $M_{n,b}$ are the number-average molecular weights of the surface-bound and bulk polymer, respectively, and ξ is a function representing the effects of confinement on surface-initiated polymerization. ξ depends on grafting density, substrate geometry, the polymerization mechanism, and other factors. Keeping these ideas in mind, the bulk simulation results are plotted in Figure 2b. The bulk simulations were run at the same temperatures and initiator conversions as the "grafting from" experiments.

The thickness of a neutral polymer brush depends on polymer molecular weight and the polymer grafting density, i.e., the number of grafted polymer chains per unit area. In the dry brush state these are related via a simple mass balance

$$d = \frac{M_{n,s}\sigma_p}{\rho N_A} \quad (3)$$

where d is dry brush thickness, σ_p is areal polymer grafting density, ρ is density (constant for this system), and N_A is Avogadro's constant. Prucker and Rühe[42] showed that for SI-

dx.doi.org/10.1021/ma300491e | Macromolecules 2012, 45, 3802−3815

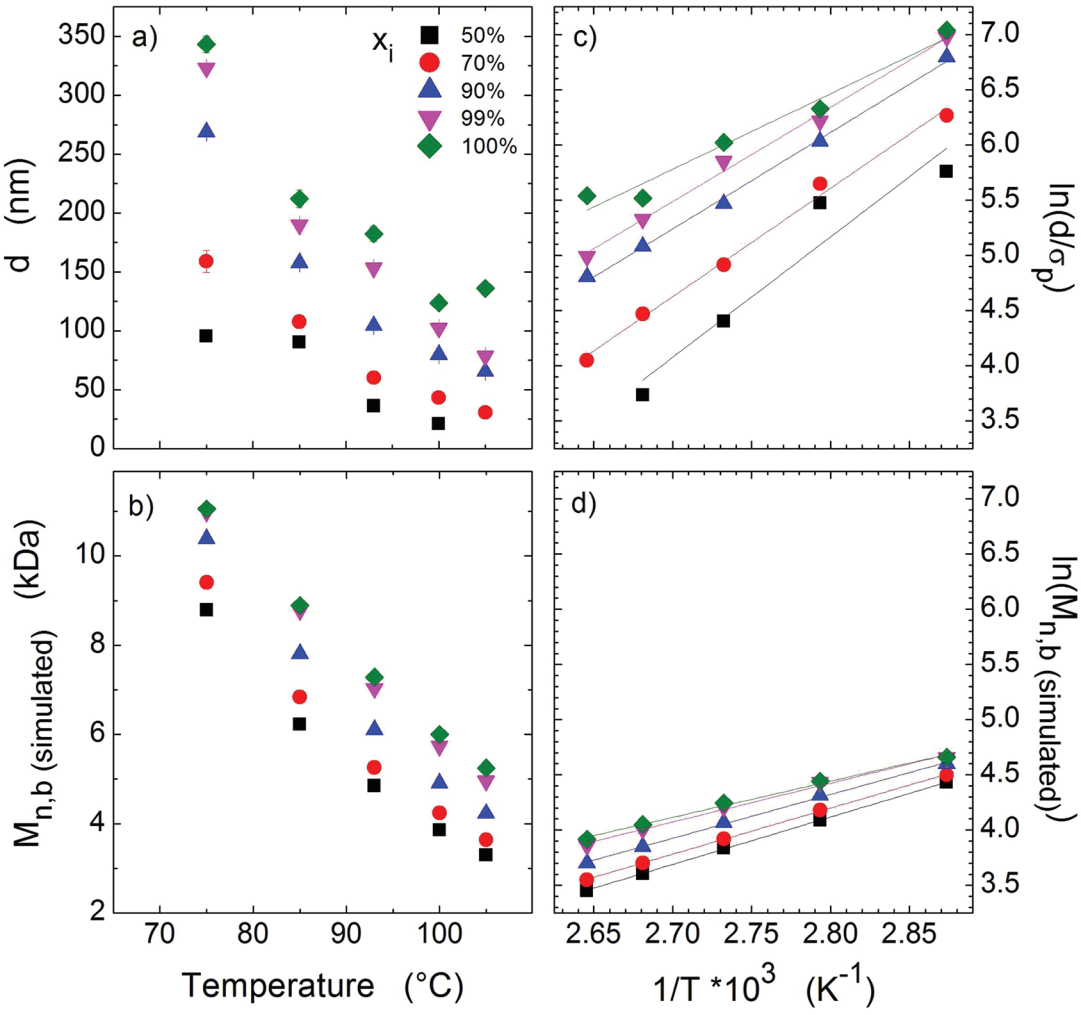

Figure 2. Properties of polystyrene formed by free-radical polymerization at varying temperatures and initiator conversions x_i: (a) dry thickness d of PS brushes on silicon wafers grown from BAIN, (b) simulated bulk number-average molecular weight $M_{n,b(simulated)}$ of free polystyrene formed in solution, (c) Arrhenius plot for d divided by grafting density σ_p, estimated from eq 4, (d) Arrhenius plot for $M_{n,b(simulated)}$. Simulations were performed using Gillespie's stochastic simulation algorithm (GSSA) under conditions described in the text.

Table 3. Kinetic Parameters Used in GSSA Simulation[73,74]

	preexponential factor	activation energy (kJ/mol)
decomposition, k_d	1.58×10^{15} s^{-1}	128.9
propagation, k_p	2.16×10^{7} M^{-1} s^{-1}	32.5
termination, k_t	2.59×10^{4} M^{-1} s^{-1}	9.9

FRP of PS from silica gel the number of grafted polymers increases with increasing temperature at 50% initiator conversion. Dividing by surface area, we plot grafting density from Prucker and Rühe's data in Figure S7 of the Supporting Information and make a linear fit to estimate grafting density as a function of temperature:

$$\sigma_p\ (\mathrm{nm}^{-2}) = 0.0078T\ (\mathrm{K}) - 2.42 \quad (4)$$

Equation 4 represents only a rough approximation for our case, considering that we use a different surface geometry and cover a range of initiator conversions. Nevertheless, it underscores a key point: at a given initiator conversion, σ_p tends to increase with temperature. To understand why this occurs, consider that the polymer grafting density σ_p can be expressed as follows:

$$\sigma_p = f x_i \sigma_i \quad (5)$$

Therefore, for constant initiator conversion x_i and constant initiator grafting density σ_i, σ_p depends only on f, the fraction of initiators that succeed in creating a polymer chain. A primary influence on f is the cage effect, in which the radicals formed by initiator decomposition tend to recombine with each other unless they diffuse out of a "cage" made of solvent molecules. The cage effect is lessened as viscosity decreases, which occurs with increasing temperature. Thus, we expect f and consequently σ_p to increase with increasing temperature, as it does in eq 4.

As seen in Figure 2a, d decreases with increasing temperature at all values of x_i, even though σ_p increases as discussed above. Therefore, according to eq 3, the strong decrease in d with temperature must be due to a corresponding decrease in $M_{n,s}$. Molecular weight typically decreases with increasing temperature in FRP because of an increasing concentration of radicals, leading to faster chain termination. Next, we note that d increases with increasing x_i at a given temperature. This occurs because each grafted polymer originates from a grafted initiator molecule; as more initiator molecules are activated and form grafted polymers, the number of grafted chains per area increases. In other words, σ_p tends to increase with x_i, in agreement with eq 5. Figure 2b shows that for simulated bulk

dx.doi.org/10.1021/ma300491e | Macromolecules 2012, 45, 3802−3815

polymerization $M_{n,b}$ decreases with increasing temperature, in a qualitatively similar way to d in Figure 2a. In addition, simulated $M_{n,b}$ also increases with increasing initiator conversion. This occurs because the radical concentration tends to decrease over the course of the reaction as initiator concentration is diminished, leading to slower termination and longer instantaneous average chain length in later stages of the polymerization (recall that for continuously initiated FRP the average radical lifetime is on the order of seconds).

The behavior of bulk molecular weight with respect to temperature is described by an Arrhenius-type equation:[79]

$$\ln(M_{n,b}) = \ln\left(\frac{bA_p[M]M_0}{(fA_dA_t[I])^{1/2}}\right) - \frac{E_p - \frac{E_d + E_t}{2}}{RT} \quad (6)$$

where [M] is monomer concentration, M_0 is the monomer molecular weight, [I] is initiator concentration, b is a constant of order unity that depends on the mode of termination, A is a kinetic preexponential factor, and E is an activation energy; the subscripts p, d, and t refer to propagation, decomposition, and termination, respectively. Equation 6 is based on the concept of the kinetic chain length, which assumes that the instantaneous average degree of polymerization is proportional to the ratio of propagation rate to initiation/termination rate (which are equivalent at steady state). By substituting[80] eqs 2 and 3 into eq 6, we obtain an analogous relationship for SI-FRP which depends on grafting density and includes the function ξ to account for deviations between molecular weight of the bulk and surface-bound polymers:

$$\ln\left(\frac{d}{\sigma_p}\right) = \ln\left(\frac{\xi bA_p[M]M_0}{\rho N_A(fA_dA_t[I])^{1/2}}\right) - \frac{E_p - \frac{E_d + E_t}{2}}{RT} \quad (7)$$

Equations 6 and 7 are linear when plotted as the left-hand side against $1/T$, assuming the logarithmic term on the right-hand side is constant; this assumption breaks down if there are variations in ξ, [M], or f at constant x_i, which will be discussed below. Although the linearized equations have different intercepts, their slopes are the same. The slopes are proportional to an overall activation energy with respect to molecular weight, which we refer to here as E_A:

$$E_A = E_p - \frac{E_d + E_t}{2} \quad (8)$$

For styrene initiated by AIBN, E_A is approximately −36 kJ/mol.[73,74]

Using eq 4 to estimate σ_p in eq 7, we plot $\ln(d/\sigma_p)$ vs $1/T$ in Figure 2c. Figure 2d contains plots of $\ln(M_{n,b(simulated)})$ vs $1/T$ for the simulated bulk polymerization, according to eq 6. In both cases the plots are approximately linear for constant values of x_i between 50% and 100%, but the slopes are quite different between the two plots, contrary to what would be expected based on eqs 6 and 7. $E_{A,s}$ values calculated from the slopes of the brush plots are shown in Figure 3a, and $E_{A,b(simulated)}$ from the simulated $M_{n,b}$ plots are in Figure 3b. The trends are qualitatively similar, with E_A trending towards zero as x_i is increased in both cases. The variation in E_A with x_i for both plots is primarily due to the fact that monomer conversion varies with temperature and x_i, contrary to the assumption of constant [M] at constant x_i in eqs 6 and 7. A further cause of variation in E_A with x_i is that, in both real and simulated polymerizations, what is measured is not the instantaneous

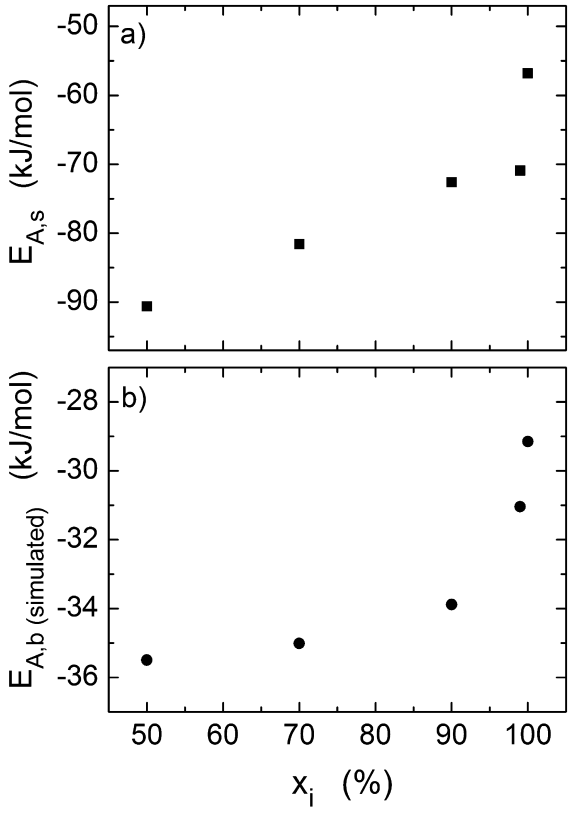

Figure 3. Apparent overall FRP activation energies: (a) $E_{A,s}$, activation energy based on thickness of PS brushes divided by grafting density, and (b) $E_{A,b(simulated)}$, activation energy based on simulated $M_{n,b}$ of bulk polystyrene. $E_{A,s}$ and $E_{A,b(simulated)}$ are calculated from slopes of Arrhenius plots in Figures 2c and 2d, respectively, using eqs 6 and 7.

average length (or thickness) of the polymer for which eqs 6 and 7 are derived, but rather a cumulative average of all instantaneous lengths (or thicknesses) over the time of reaction. Despite these variations, $E_{A,b(simulated)}$ values for the simulated bulk polymerization are near the theoretical value of −36 kJ/mol at 50% x_i and increase to −29 kJ/mol as x_i is increased to 100%. On the other hand, apparent $E_{A,s}$ values for the surface polymerization are significantly greater and cover a broader range, varying from −91 kJ/mol at 50% initiator conversion to −56 kJ/mol at 100% initiator conversion. Therefore, we find that apparent E_A values for surface and bulk polymerizations are not the same, as had been expected according to eqs 6 and 7.

What causes $E_{A,s}$ to be apparently greater for SI-FRP than the theoretical E_A value for FRP in solution? It is unlikely that the activation energies change simply due to confinement effects in surface-initiated polymerization. Therefore, the shift in slope must be due to temperature dependence of some factor(s) in the logarithmic term on the right-hand side of eq 7. For example, in SI-FRP $M_{n,s}$ has been found to depend on a so-called two-dimensional Trommsdorff effect (2DTE).[42,63,65] This effect is summarized as follows: Since SI-FRP takes place in a small flat volume near the surface, the polymerization environment can quickly become viscous as the thin brush layer fills up with dead polymer chains. As new polymers are formed in this viscous environment, translational diffusion is inhibited and termination is slowed, causing the average degree of polymerization to increase. The 2DTE occurs much earlier in time than the traditional Trommsdorff effect in bulk polymer-

dx.doi.org/10.1021/ma300491e | Macromolecules 2012, 45, 3802−3815

ization, since it does not depend on viscosity of the bulk solution. All other factors being equal, the 2DTE causes $M_{n,s}$ to increase independently of $M_{n,b}$, which is equivalent to saying that ξ increases.[81] The 2DTE becomes greater in magnitude as $1/T$ increases because viscosity increases due to both an increase in polymer molecular weight and a decrease in temperature. The result is greater slopes of the Arrhenius plots, as observed for our polymer brush data. We stress again that these observations do not imply that the activation energies of the FRP processes are affected by initiating polymerization from a substrate; rather, the observed shift in apparent $E_{A,s}$ is actually an effect of temperature on ξ. Other effects that may influence the slopes of the Arrhenius curves but are not captured by eq 7 include chain transfer, local monomer concentration in the brush, and polydispersity of the surface-bound polymer.

To compare the performance of BAIN with ester-containing azo initiators, we formed PS brushes by SI-FRP using AEMS and AETS. Figure 4 compares the thickness of brushes grown

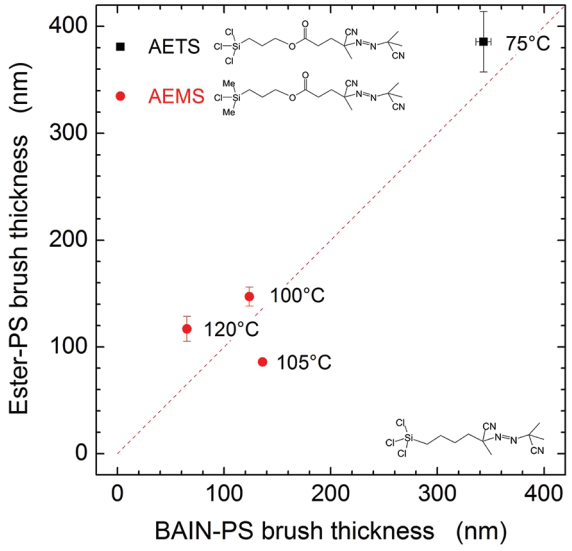

Figure 4. Dry thickness of polystyrene brushes formed by SI-FRP from azo initiators containing ester linkers (schematically pictured next to legend), compared with polystyrene brushes formed by BAIN (schematically pictured above abscissa), at various temperatures. All samples are at 100% initiator conversion. The dotted line corresponds to $y = x$.

from ester containing initiators with those formed by BAIN, all at 100% initiator conversion. While more experiments are clearly needed to elucidate the differences, if any, between the two initiating systems, the few samples shown representing PS brushes formed by ester initiators are comparable in thickness with those formed by BAIN at the same temperatures. This behavior is expected, since the initiators are chemically identical with the exception of the ester functional group in the linker. Since the ester is separated from the AIBN-like group of AETS and AEMS by a two-carbon spacer, it is expected and found to have no effect on the decomposition kinetics of the initiator. This is demonstrated by the fact that our DSC results indicate nearly identical kinetics for BAIN and AETS. Furthermore, it has been shown that self-assembly on an oxide substrate does not affect the decomposition kinetics of the ester-based azo initiators.[42] Finally, the number of reactive chloro groups on the silane anchor does not appear to affect significantly the thickness of the polymer brush formed, as both trichlorosilane-based AETS and dimethylchlorosilane-based AEMS generate brushes that are comparable in thickness with those formed by BAIN.

Simultaneous Bulk and Surface-Initiated Reverse Atom Transfer Radical Polymerization (RATRP). To demonstrate the general applicability of BAIN in initiating radical reactions beyond simple free radical polymerizations, we have also performed tests using reverse ATRP (RATRP) and RAFT methodologies. RATRP requires an initiator-to-catalyst ratio on the order of 1 in order to function properly.[82] Therefore, rather than trying to determine quantitatively the amount of surface-grafted initiator (typically on the order of a nmol/cm2 for a silicon wafer sample) and accurately deliver corresponding amounts of catalyst, we chose to use mM levels of catalyst and a corresponding amount of free AIBN in the bulk solution. This simultaneous bulk and surface-initiated approach allows us to accurately set the initiator-to-catalyst ratio by varying only the bulk quantities, since the small amount of surface initiator is insignificant compared with the amount of free AIBN. The drawback of this approach is that competition for monomer between propagating bulk polymers and the comparatively small amount of grafted polymers likely retards the rate of surface-initiated polymerization and the resulting brush molecular weight.[46] Nevertheless, the simultaneous bulk and surface-initiated method is effective at forming both free and grafted polymer by RATRP.[54] The brush layer formed by SI-RATRP is easily separated from the bulk polymer by removing the substrate from solution and rinsing in a good solvent. Two silicon wafers, one functionalized with BAIN and the other with AETS, were inserted in a solution containing styrene (3.77 M), $CuBr_2$ (0.43 mM), PMDETA (0.65 mM), and AIBN (0.357 mM) in anisole, and the solution was degassed. The solution was heated under argon for 23 h at 100 °C, which is sufficient to achieve 100% conversion of the azo initiators. The substrates were removed and rinsed with methanol/water to remove the copper catalyst and with toluene to remove adsorbed free polystyrene. As seen in Figure 5, the thickness of the brush layers after RATRP in styrene was 20−30 nm as measured by ellipsometry. Since the brushes were generated by a "living" polymerization, they remain end-capped with bromine groups, enabling them act as a macroinitiator. For example, grafted block copolymers can be formed by subjecting the grafted macroinitiator substrates to standard ATRP in solution of another monomer. To demonstrate this effect, we stored the substrates in the dark for a few hours and then inserted them in a degassed solution containing MMA (4 M), CuBr (11 mM), and PMDETA (22 mM) in anisole. The solution was heated under argon for 24 h at 100 °C, after which the substrates were rinsed with methanol/water and toluene. The brush thicknesses as measured by ellipsometry were roughly double those from before insertion in the MMA solution. This result confirms that the initial polystyrene layer acts as a macroinitiator for ATRP of MMA, forming grafted block copolymers. Therefore, we conclude that the polystyrene was formed by SI-RATRP.

To further investigate the properties of the grafted block copolymers, we observed the changes in wettability of the substrates after each polymerization step and following immersion in a selective solvent for each block. Figure 5 depicts water contact angles measured on PS and PS-*b*-PMMA grafts for both series of initiators, i.e., BAIN (Figure 5a) and AETS (Figure 5b). It is known that PS-*b*-PMMA block

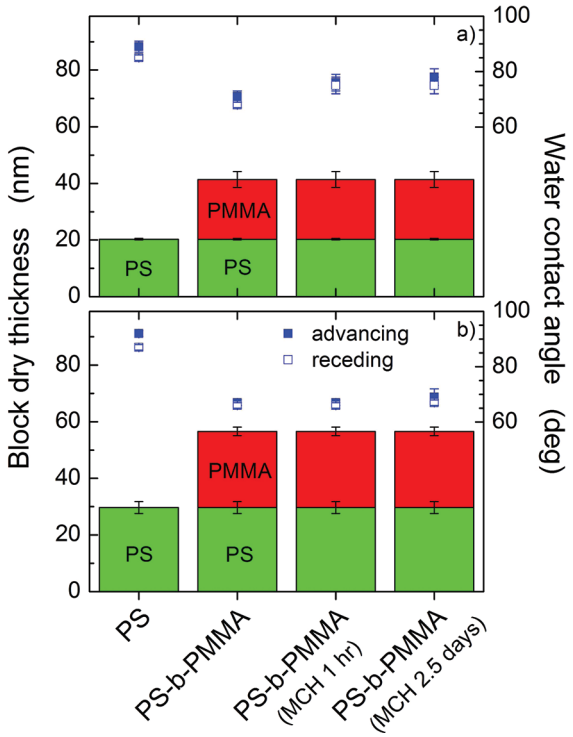

Figure 5. Dry thickness (left ordinate) and water contact angle (advancing: closed symbols; receding: open symbols; right ordinate) of PS, PS-*b*-PMMA brushes on flat silica substrates grown from (a) BAIN and (b) AETS initiators in as-prepared form and after treatment with methylcyclohexane (MCH) for 1 h and 2.5 days.

copolymers undergo reversible conformational reorganization when immersed in selective solvents; this surface reorientation can be measured by a reversible change in water contact angle. The samples were immersed in methylcyclohexane (MCH), a selective solvent for PS, first for 1 h and then for 2.5 days. Unlike in previous studies,[67] water contact angles for our block copolymer samples did not return completely to those for pure PS following immersion in MCH. We have to note, however, that the DI water contact angles in BAIN-based samples did increase to an intermediate value between that for pure PS (≈89°) and pure PMMA (≈68°). The reason why the system did not exhibit a completely switchable behavior is that our samples have PMMA blocks roughly equivalent in thickness (21–27 nm) to the PS blocks (20–30 nm). Grafted block copolymers have been found to change wettability reversibly only when the top block is significantly shorter than the bottom block.[15] In cases where the top (PMMA) block is significantly thinner than the bottom (PS) block, the short top block is able to reorient and expose the longer bottom block at the surface. If, in contrast, the top block longer than or equal to the length of the bottom block, the top block is prevented from reorienting due to conformational constraints and the bottom block is unable to stretch far enough to cover a large top block. In our experiment the AETS block copolymer sample is in this nonresponse regime, while the BAIN block copolymer with its shorter PMMA block is in a partial-response regime.

Surface-Initiated Reversible Addition–Fragmentation Transfer (SI-RAFT). Polystyrene brushes were also formed from BAIN by RAFT polymerization, using 2-cyano-2-propyl-dodecyltrithiocarbonate as a chain transfer agent (CTA). Silicon wafers functionalized with BAIN were placed in vials containing a 1/1 (v/v) mixture of styrene and toluene and varying concentrations of the CTA. No free AIBN was added to the RAFT solutions. The vials were heated under argon for 18 h at 70 °C, corresponding to about 93% initiator conversion. Figure 6a depicts the dependence of PS dry brush thickness *d*

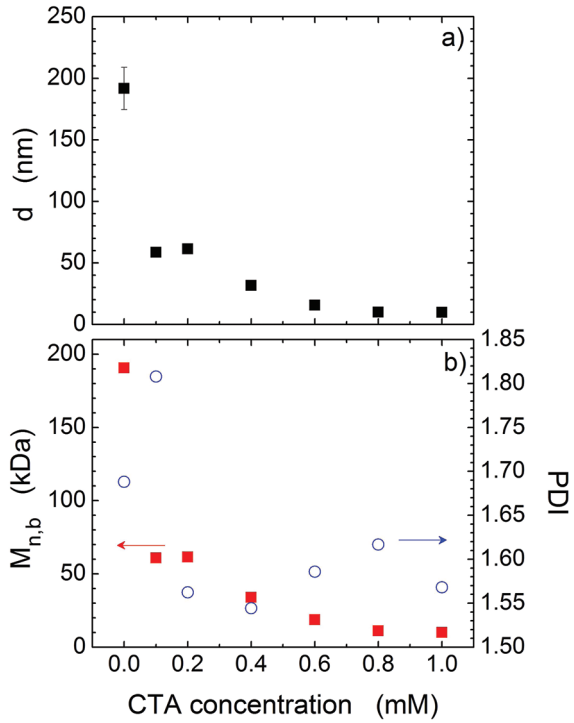

Figure 6. (a) Dry thickness *d* of PS brushes and (b) number-average molecular weight ($M_{n,b}$ closed red squares, left ordinate) and polydispersity index (PDI, open circles, right ordinate) of bulk-grown polymer grown from BAIN initiator on flat substrates by RAFT as a function of CTA concentration.

measured by ellipsometry as a function of the CTA concentration. A control SI-FRP sample which was formed at 70 °C for 23 h (≈97% initiator conversion) is included at CTA = 0. The results shown in Figure 6b, obtained from size exclusion chromatography (SEC) of the bulk solution from each vial, include the bulk number-average molecular weight ($M_{n,b}$, red closed squares) and bulk polydispersity index (PDI, blue open circles). The corresponding SEC traces are shown in Figure S8 of the Supporting Information. We again refer to eq 2 and emphasize that the characteristics of polymers formed in bulk are not the same as those grown on the surface, and therefore the SEC data should not be considered indicative of the properties of the grafted polymer. Both *d* and $M_{n,b}$ decrease with increasing CTA concentration. This is consistent with increasing the fraction of dormant polymers due to increased concentration of CTA, resulting in a shorter average chain length. The brush thickness and bulk molecular weight of the FRP-based polymer are much higher than those formed by RAFT, indicating that the CTA exhibits a strong effect over the rate polymerization. On the other hand, the PDI of the bulk polymer does not show a similar decrease but instead remains fairly consistent at most values of CTA concentration, reaching a minimum value of 1.55 at 0.4 mM CTA. The measured bulk PDI are higher than those typically reported for RAFT polymerization, but all are lower than the PDI of FRP except at the very lowest CTA concentration. FRP can theoretically have a PDI as low as 1.5, but only if termination occurs

dx.doi.org/10.1021/ma300491e | *Macromolecules* 2012, 45, 3802–3815

exclusively by radical recombination. The fact that bulk PDI does not decrease with increasing polymer thickness suggests an optimum CTA concentration for achieving thick polymer layers with a relatively well-controlled molecular weight distribution.

Brush Stability. To test the stability of brushes formed by BAIN, which are linked to the substrate only by C−C bonds, we first performed a typical procedure used to degraft brushes for analysis. Degrafting and subsequent analysis by SEC is one of the most reliable methods for characterizing polymers formed by the "grafting from" method. However, the quantity of surface-initiated polymer obtained from planar substrates is typically not sufficient for analysis by conventional SEC detectors; hence, degrafting is only useful for particulate substrates with high surface area. In this study we did not collect the degrafted chains but merely measured the resulting thickness to determine the extent of brush cleavage. Figure 7

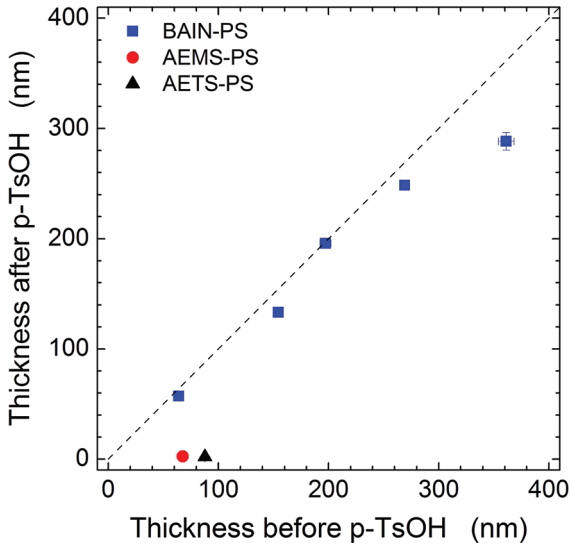

Figure 7. Dry thickness of SI-FRP polystyrene brushes after refluxing overnight in a toluene/10% methanol solution of *p*-toluenesulfonic acid as a function of initial dry thickness. The dotted line corresponds to $y = x$.

shows the thickness of SI-FRP PS brushes measured by ellipsometry before and after refluxing overnight in a solution of *p*-toluenesulfonic acid (*p*-TsOH) in toluene/10% methanol. The thickness of PS brushes formed from AEMS and AETS decreased by nearly 100%, which is consistent with complete transesterification of the ester linkers in both cases. The decrease in thickness for BAIN-based brushes was in the range of 1−20%, likely owing to partial cleavage of the Si−O−Si bonds tethering the brushes to the surface. Nevertheless, in general, BAIN forms brushes that are much more stable to *p*-TsOH treatment than ester-based brushes.

Besides these relatively harsh conditions, we have also tested stability under normal aqueous conditions for polyelectrolyte brushes. A drawback of having esters in the linker structure is that esters are susceptible to hydrolysis in aqueous environments at varying conditions of pH. This becomes more of an issue when grafted polymers are under tension, since mechanical force tends to increase rates of reactions such as hydrolysis. Densely grafted polymer brushes inherently experience tension due to the unfavorable excluded volume effect resulting in stretched conformation of the chains; this tension can be amplified by interchain repulsions such as electrostatic forces among charged polyelectrolytes. We present here examples of selected experiments comparing the stability of weak and strong polycationic brushes, grafted using either BAIN or an ester-containing initiator, in this case the common ATRP initiator [11-(2-bromo-2-methyl)propionyloxy]-undecyltrichlorosilane (BMPUS). More detailed discussion will be provided in a separate publication.[75]

Polyelectrolytes can be classified as either weak polyelectrolytes, whose degree of charging varies as a function of solution pH, or strong polyelectrolytes, whose degree of charging is constant over a normal range of pH. Poly(2-(dimethylamino)ethyl methacrylate) (PDMAEMA) is an example of a weak cationic polyelectrolyte, with a bulk pK_a of ≈7.5. The amine groups in PDMAEMA can be quaternized to form a strong polycation, which we refer to here as qPDMAEMA. We formed PDMAEMA brushes via two different methods: SI-FRP from BAIN and SI-ATRP from BMPUS, both on silicon wafers. Selected PDMAEMA brush samples from both BAIN and BMPUS were then heated in a solution of excess methyl iodide. Thickness of the brushes increased after the treatment, indicating the formation of quaternary ammonium side groups in the brush. PDMAEMA and qPDMAEMA brushes were then incubated in phosphate buffered saline solutions at pH values of 4, 7.4, and 9, for periods ranging from 1 to 5 days. The dry thickness of the brushes following incubation was measured by spectroscopic ellipsometry, and the results normalized by initial thickness (before incubation) are plotted in Figure 8.

The thickness of the BAIN-based PDMAEMA brushes did not change significantly after incubation in the PBS solution, regardless of the pH. The thickness of PDMAEMA brushes grafted by the ester-based BMPUS was essentially constant at

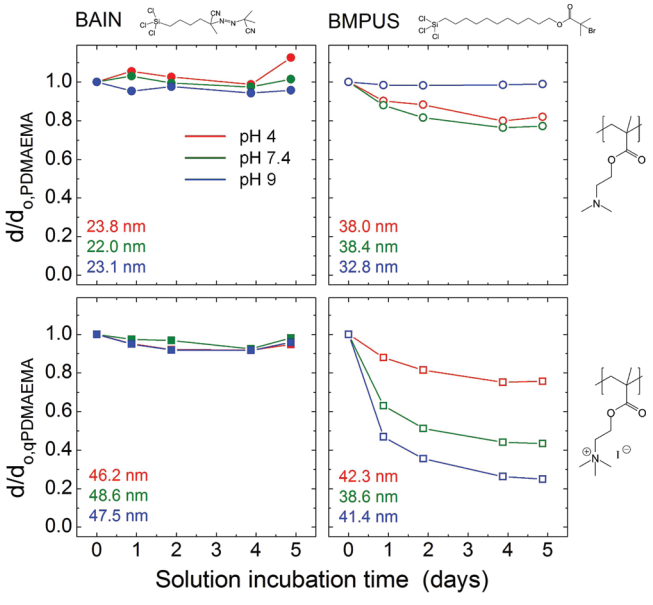

Figure 8. Relative dry thickness d/d_0 of poly(2-(dimethylamino)ethyl methacrylate) (PDMAEMA) brushes (circles) and quaternized PDMAEMA brushes (squares) formed by SI-FRP from BAIN (closed symbols), and by SI-ATRP from ester-based BMPUS (open symbols), as a function of incubation time in phosphate buffer solution of pH 4 (red), pH 7.4 (green), and pH 9 (blue). Initial thicknesses d_0 of the samples are indicated in the lower left corner of each pane, color coded according to the pH of the solution the sample was incubated in.

dx.doi.org/10.1021/ma300491e | *Macromolecules* 2012, 45, 3802−3815

pH 9, but decreased by ≈18% at pH 4 and ≈23% at pH 7.4. This, at first glance, confusing behavior can be explained by considering two competing mechanisms that take place in this system. First, the ester hydrolysis reaction is catalyzed by hydroxide ions; therefore, the rate of hydrolysis increases as pH increases. Second, the brush transitions from neutral to positively charged as the solution becomes acidic; therefore, the tension on the brush due to electrostatic repulsions increases as pH decreases. Both charging (tension) and hydroxide concentration tend to accelerate hydrolysis of the ester linker, resulting in degrafting of brush chains. At pH 9 the hydroxide concentration is the highest, but the brush is not charged; therefore, the tension is minimized and no degrafting occurs. At pH 4 very few hydroxide ions are available, but the brush is highly charged which induces tension that leads to moderate degrafting. At pH 7.4 both of the contributions to degrafting are balanced; hydroxide ion concentration is moderate, and the brush is partially charged.[83] We detect maximum degrafting at pH 7.4 due to the combination of base-catalyzed hydrolysis and tension resulting from partial charging of the brush.

The thickness of qPDMAEMA brushes grafted from BAIN also does not decrease significantly over 5 days of incubation in PBS, regardless of pH. However, BMPUS-based qPDMAEMA brushes degrafted more than their corresponding PDMAEMA brushes, and the extent of degrafting increases with increasing pH. At pH 4, ester-based qPDMAEMA thickness decreases by ≈24%, compared with ≈57% at pH 7.4 and ≈75% at pH 9. These results agree well with the explanation presented above. Since qPDMAEMA is a strong polyelectrolyte, its degree of charging is not influenced by pH, and hence the tension on the brush remains approximately constant in each of the PBS solutions. As hydroxide concentration increases the rate of ester hydrolysis increases, and therefore we see increased degrafting as pH increases. We point out that at pH 4 the rates of degrafting of PDMAEMA and qPDMAEMA brushes are similar, because both the strong and weak polycations are highly charged at pH 4 and hence the tension is comparable. On the other hand, at pH 7.4 and 9, the degree of charging depends strongly on whether or not the brush is quaternized, which leads to very different rates of degrafting. These observations emphasize the role of charges on regulating tension on the brush linker and the subsequent rate of degrafting by ester hydrolysis. BAIN-based brushes do not degraft at any of the conditions studied, clearly illustrating the superior stability of the nonester-based initiator. An in-depth investigation of these and other factors influencing polymer brush stability is forthcoming.[75]

CONCLUSIONS

In this work we have demonstrated the synthesis of a novel AIBN-type radical initiator for performing surface-initiated radical polymerizations. The so-called BAIN initiator contains only carbon−carbon bonds between the surface and the initiating group, in contrast to typical surface-bound initiators that feature esters or amides in the linking structure. As a result, the BAIN initiator produces grafted polymer brushes whose stability is considerably greater than that of ester-based brushes, under a variety of conditions including harsh acid treatment as well as relatively mild aqueous solutions. The synthesis of the initiator represents an improvement over previous methods in terms of yield and safety, with a significant decrease in the amount of cyanide usage. The kinetics of the initiator agree very well with those of previously used AIBN-type initiators, and the thickness of polystyrene brush formed by SI-FRP is comparable with those formed using ester-containing azo initiators. The Arrhenius behavior of SI-FRP differs from that of FRP in the bulk, likely owing to diffusion limitations within the brush that slow termination. The growth of polymer brushes by RATRP and RAFT demonstrates the versatility of the initiator; not only can it be used to initiate free-radical polymerization, but it can also be employed in "living" radical polymerization methods.

ASSOCIATED CONTENT

Supporting Information

Synthesis details, FT-IR and ^{1}H NMR spectra of synthetic intermediates, XPS spectra of BAIN self-assembled layers on silicon, details of initiator grafting density calculation, DSC trace of AETS, details of decomposition kinetics, details of polymer grafting density calculation, SEC traces of bulk polymer from RAFT experiments. This material is available free of charge via the Internet at http://pubs.acs.org.

AUTHOR INFORMATION

Corresponding Author

*E-mail: Jan_Genzer@ncsu.edu.

Present Address

$^{\perp}$Department of Chemical & Biomolecular Engineering, University of California, Berkeley, CA 94720.

Notes

The authors declare no competing financial interest.

ACKNOWLEDGMENTS

This work was supported by the National Science Foundation (Grant DMR-0906572). Partial support from the Army Research Office (Grant W911NF-04-D0003-0016) is also appreciated.

REFERENCES

(1) Zhang, Z.; Finlay, J. A.; Wang, L.; Gao, Y.; Callow, J. A.; Callow, M. E.; Jiang, S. *Langmuir* **2009**, *25*, 13516−13521.
(2) Tugulu, S.; Klok, H.-A. *Biomacromolecules* **2008**, *9*, 906−912.
(3) Hucknall, A.; Rangarajan, S.; Chilkoti, A. *Adv. Mater.* **2009**, *21*, 2441−2446.
(4) Dalsin, J. L.; Messersmith, P. B. *Mater. Today* **2005**, *8*, 38−46.
(5) Yang, W. J.; Cai, T.; Neoh, K.-G.; Kang, E.-T.; Dickinson, G. H.; Teo, S. L.-M.; Rittschof, D. *Langmuir* **2011**, *27*, 7065−7076.
(6) Fristrup, C. J.; Jankova, K.; Hvilsted, S. *Soft Matter* **2009**, *5*, 4623.
(7) Xu, F. J.; Cai, Q. J.; Li, Y. L.; Kang, E. T.; Neoh, K. G. *Biomacromolecules* **2005**, *6*, 1012−1020.
(8) Huang, J.; Li, X.; Zheng, Y.; Zhang, Y.; Zhao, R.; Gao, X.; Yan, H. *Macromol. Biosci.* **2008**, *8*, 508−515.
(9) Yu, K.; Kizhakkedathu, J. N. *Biomacromolecules* **2010**, *11*, 3073−3085.
(10) Barbey, R.; Kauffmann, E.; Ehrat, M.; Klok, H.-A. *Biomacromolecules* **2010**, *11*, 3467−3479.
(11) Dong, R.; Krishnan, S.; Baird, B. a; Lindau, M.; Ober, C. K. *Biomacromolecules* **2007**, *8*, 3082−3092.
(12) Luzinov, I.; Minko, S.; Tsukruk, V. V. *Soft Matter* **2008**, *4*, 714−725.
(13) Stuart, M. A. C.; Huck, W. T. S.; Genzer, J.; Müller, M.; Ober, C.; Stamm, M.; Sukhorukov, G. B.; Szleifer, I.; Tsukruk, V. V.; Urban, M.; Winnik, F.; Zauscher, S.; Luzinov, I.; Minko, S. *Nat. Mater.* **2010**, *9*, 101−113.
(14) Motornov, M.; Minko, S.; Eichhorn, K.-J.; Nitschke, M.; Simon, F.; Stamm, M. *Langmuir* **2003**, *19*, 8077−8085.

(15) Xu, C.; Wu, T.; Drain, C. M.; Batteas, J. D.; Fasolka, M. J.; Beers, K. L. *Macromolecules* **2006**, *39*, 3359−3364.
(16) Kaholek, M.; Lee, W.-K.; LaMattina, B.; Caster, K. C.; Zauscher, S. *Nano Lett.* **2004**, *4*, 373−376.
(17) Granville, A. M.; Boyes, S. G.; Akgun, B.; Foster, M. D.; Brittain, W. J. *Macromolecules* **2004**, *37*, 2790−2796.
(18) Jhon, Y. K.; Bhat, R. R.; Jeong, C.; Rojas, O. J.; Szleifer, I.; Genzer, J. *Macromol. Rapid Commun.* **2006**, *27*, 697−701.
(19) Jones, D. M.; Smith, J. R.; Huck, W. T. S.; Alexander, C. *Adv. Mater.* **2002**, *14*, 1130.
(20) Balamurugan, S.; Mendez, S.; Balamurugan, S. S.; O'Brie, M. J.; López, G. P. *Langmuir* **2003**, *19*, 2545−2549.
(21) Plunkett, K. N.; Zhu, X.; Moore, J. S.; Leckband, D. E. *Langmuir* **2006**, *22*, 4259−4266.
(22) Nagase, K.; Kobayashi, J.; Kikuchi, A.; Akiyama, Y.; Kanazawa, H.; Okano, T. *Langmuir* **2011**, *27*, 10830−10839.
(23) Jonas, A. M.; Glinel, K.; Oren, R.; Nysten, B.; Huck, W. T. S. *Macromolecules* **2007**, *40*, 4403−4405.
(24) Zhou, F.; Shu, W.; Welland, M. E.; Huck, W. T. S. *J. Am. Chem. Soc.* **2006**, *128*, 5326−5327.
(25) Bittrich, E.; Kuntzsch, M.; Eichhorn, K.-J.; Uhlmann, P. *J. Polym. Sci., Polym. Phys.* **2010**, *48*, 1606−1615.
(26) Ito, Y.; Ochiai, Y.; Park, Y. S.; Imanishi, Y. *J. Am. Chem. Soc.* **1997**, *119*, 1619−1623.
(27) Tokareva, I.; Minko, S.; Fendler, J. H.; Hutter, E. *J. Am. Chem. Soc.* **2004**, *126*, 15950−15951.
(28) Uline, M. J.; Rabin, Y.; Szleifer, I. *Langmuir* **2011**, *27*, 4679−4689.
(29) Schüwer, N.; Klok, H.-A. *Langmuir* **2011**, *27*, 4789−4796.
(30) Zhou, F.; Biesheuvel, P. M.; Choi, E.-Y.; Shu, W.; Poetes, R.; Steiner, U.; Huck, W. T. S. *Nano Lett.* **2008**, *8*, 725−730.
(31) Lomadze, N.; Kopyshev, A.; Rühe, J.; Santer, S. *Macromolecules* **2011**, *44*, 7372−7377.
(32) Ouyang, H.; Xia, Z.; Zhe, J. *Nanotechnology* **2009**, *20*, 195703.
(33) Minko, S. In *Polymer Surfaces and Interfaces Characterization, Modification and Applications*; Stamm, M., Ed.; Springer-Verlag: Berlin, 2008; pp 215−234.
(34) Rühe, J.; Knoll, W. *J. Macromol. Sci., Polym. Rev.* **2002**, *32*, 91−138.
(35) Zhao, B.; Brittain, W. J. *Prog. Polym. Sci.* **2000**, *25*, 677−710.
(36) Matyjaszewski, K.; Miller, P. J.; Shukla, N.; Immaraporn, B.; Gelman, A.; Luokala, B. B.; Siclovan, T. M.; Kickelbick, G.; Vallant, T.; Hoffmann, H.; Pakula, T. *Macromolecules* **1999**, *32*, 8716−8724.
(37) Edmondson, S.; Osborne, V. L.; Huck, W. T. S. *Chem. Soc. Rev.* **2004**, *33*, 14−22.
(38) Takahashi, H.; Nakayama, M.; Yamato, M.; Okano, T. *Biomacromolecules* **2010**, *11*, 1991−1999.
(39) Baum, M.; Brittain, W. J. *Macromolecules* **2002**, *35*, 610−615.
(40) Prucker, O.; Rühe, J. *Langmuir* **1998**, *14*, 6893−6898.
(41) Prucker, O.; Rühe, J. *Macromolecules* **1998**, *31*, 592−601.
(42) Prucker, O.; Rühe, J. *Macromolecules* **1998**, *31*, 602−613.
(43) Ashford, E. J.; Naldi, V.; O'Dell, R.; Billingham, N. C.; Armes, S. P. *Chem. Commun.* **1999**, 1285−1286.
(44) Genzer, J. *Macromolecules* **2006**, *39*, 7157−7169.
(45) Turgman-Cohen, S.; Genzer, J. *Macromolecules* **2010**, *43*, 9567−9577.
(46) Turgman-Cohen, S.; Genzer, J. *J. Am. Chem. Soc.* **2011**, *133*, 17567−17569.
(47) Zhang, J.; Yang, Y.; Zhao, C. *J. Polym. Sci., Polym. Chem.* **2007**, *45*, 5329−5338.
(48) Santer, S.; Rühe, J. *Polymer* **2004**, *45*, 8279−8297.
(49) Sidorenko, A.; Minko, S.; Schenk-Meuser, K.; Duschner, H.; Stamm, M. *Langmuir* **1999**, *15*, 8349−8355.
(50) Olivier, A.; Meyer, F.; Raquez, J.-M.; Damman, P.; Dubois, P. *Prog. Polym. Sci.* **2012**, *37*, 157−181.
(51) Chen, T.; Amin, I.; Jordan, R. *Chem. Soc. Rev.* **2012**, DOI: 10.1039/c2cs15225h.
(52) Barbey, R.; Lavanant, L.; Paripovic, D.; Schüwer, N.; Sugnaux, C.; Tugulu, S.; Klok, H.-A. *Chem. Rev.* **2009**, *109*, 5437−5527.
(53) Rühe, J. In *Polymer Brushes*; Advincula, R. C., Brittain, W. J., Castere, K. C., Rühe, J., Eds.; Wiley-VCH: Weinheim, 2004; pp 1−28.
(54) Ye, P.; Dong, H.; Zhong, M.; Matyjaszewski, K. *Macromolecules* **2011**, *44*, 2253−2260.
(55) Velten, U.; Shelden, R. a.; Caseri, W. R.; Suter, U. W.; Li, Y. *Macromolecules* **1999**, *32*, 3590−3597.
(56) Wang, Y.; Pei, X.; Yuan, K. *Mater. Lett.* **2005**, *59*, 520−523.
(57) Yoshikawa, C.; Goto, A.; Tsujii, Y.; Fukuda, T.; Yamamoto, K.; Kishida, A. *Macromolecules* **2005**, *38*, 4604−4610.
(58) Farquet, P.; Padeste, C.; Solak, H. H.; Gürsel, S. A.; Scherer, G. G.; Wokaun, A. *Macromolecules* **2008**, *41*, 6309−6316.
(59) Meier, L. P.; Shelden, R. A.; Caseri, W. R.; Suter, U. W. *Macromolecules* **1994**, *27*, 1637−1642.
(60) Patton, D. L.; Page, K. A.; Xu, C.; Genson, K. L.; Fasolka, M. J.; Beers, K. L. *Macromolecules* **2007**, *40*, 6017−6020.
(61) Schmelmer, U.; Paul, A.; Küller, A.; Steenackers, M.; Ulman, A.; Grunze, M.; Gölzhäuser, A.; Jordan, R. *Small* **2007**, *3*, 459−465.
(62) Prucker, O.; Habicht, J.; Park, I.-J.; Rühe, J. *Mater. Sci. Eng., C* **1999**, *8*−*9*, 291−297.
(63) Boven, G.; Oosterling, M. L. C. M.; Challa, G.; Schouten, A. J. *Polymer* **1990**, *31*, 2377−2383.
(64) Huber, D. L.; Manginell, R. P.; Samara, M. a; Kim, B.-I.; Bunker, B. C. *Science* **2003**, *301*, 352−354.
(65) Rotzoll, R.; Vana, P. *Aust. J. Chem.* **2009**, *62*, 1473−1478.
(66) Hoffmann, F.; Wolff, T. *J. Colloid Interface Sci.* **2008**, *322*, 434−447.
(67) Sedjo, R. a.; Mirous, B. K.; Brittain, W. J. *Macromolecules* **2000**, *33*, 1492−1493.
(68) McCrackin, F. L.; Passaglia, E.; Stromberg, R. R.; Steinberg, H. L. *J. Res. Natl. Bur. Stand., Sect. A* **1963**, *67A*, 363−377.
(69) Wasserman, S. R.; Tao, Y. T.; Whitesides, G. M. *Langmuir* **1989**, *5*, 1074−1087.
(70) Tillman, N.; Ulman, A.; Schildkraut, J. S.; Penner, T. L. *J. Am. Chem. Soc.* **1988**, *110*, 6136−6144.
(71) Day, A. C. *Org. Synth.* **1970**, *50*, 3.
(72) Lu, J.; Zhang, H.; Yang, Y. *Macromol. Theor. Simul.* **1993**, *2*, 747−760.
(73) Dixon, K. W. In *Polymer Handbook*; Brandrup, J., Immergut, E. H., Grulke, E. A., Abe, A., Bloch, D. R., Eds.; John Wiley & Sons: New York, 2005; pp II/2−II/4.
(74) Kamachi, M.; Yamada, B. In *Polymer Handbook*; Brandrup, J., Immergut, E. H., Grulke, E. A., Abe, A., Bloch, D. R., Eds.; John Wiley & Sons: New York, 2005; pp II/88−II/89.
(75) Galvin, C. J.; Bain, E. D.; Özçam, A. E.; Henke, A.; Šrogl, J.; Szleifer, I. S.; Genzer, J. Manuscript in preparation.
(76) Estimated monolayer thicknesses are based on simple geometric calculations of the length of the fully extended molecule, assuming the organosilane stands normal to the surface.
(77) Torfs, J. C. M.; Deij, L.; Dorrepaal, A. J.; Heijens, J. C. *Anal. Chem.* **1984**, *56*, 2863−2867.
(78) Gillespie, D. T. *J. Phys. Chem.* **1977**, *81*, 2340−2361.
(79) Odian, G. *Principles of Polymerization*, 4th ed.; Wiley: Hoboken, NJ, 2004; p 274.
(80) We note that $M_{n,b}$ in eq 6 is an instantaneous average molecular weight, whereas $M_{n,b}$ and $M_{n,s}$ in eqs 2 and 3 are averages over all reaction time. While instantaneous and time-averaged values are used interchangeably here for the sake of simplicity, they are not strictly equivalent. One implication of this discrepancy is pointed out in the discussion pertaining to Figure 3.
(81) For SI-FRP, ξ can be greater or less than unity. For example, in ref 42 on silica gel it was found that $M_{n,s} < M_{n,b}$ early in the polymerization, but $M_{n,s} > M_{n,b}$ later in the same polymerization. $M_{n,s}$ increased steadily while $M_{n,b}$ was approximately constant over the course of the polymerization.
(82) Xia, J.; Matyjaszewski, K. *Macromolecules* **1997**, *30*, 7692−7696.
(83) Although one would expect ∼50% charging since pH is near the pK_a, this would assume that the surface pK_a is equivalent to the bulk pK_a. We note, however, that the values may be different, as shown by Szleifer and co-workers in ref 84.

(84) Gong, P.; Wu, T.; Genzer, J.; Szleifer, I. *Macromolecules* **2007**, *40*, 8765−8773.